# Space-time correlations in two subsonic jets using dual-PIV measurements

Vincent Fleury*
*ONERA, 92322 Châtillon, France*

Christophe Bailly†, Daniel Juvé‡, Marc Michard§ and Emmanuel Jondeau¶
*Ecole Centrale de Lyon & CNRS, 69134 Ecully, France*

**Dual Particule Image Velocimetry (dual-PIV) measurements have been performed to investigate the space-time correlations in two subsonic isothermal round jets at Mach numbers 0.6 and 0.9. Measurements are obtained along the centerline and the shear-layer region which are closely connected with the noise generation. Integral scales have been calculated with as much as 2000 samples which provides high-quality data. The correlation scales are given in function of appropriate references, namely the local momentum thickness (respectively the jet diameter) for the shear-layer (respectively the jet axis) and the mean or rms local velocity. Far enough downstream in the shear-layer, some of the ratios between the space scales and between the time scales are relatively close to the values expected in isotropic an homogeneous turbulence. Furthermore, the relation between the time and space scales follows well the Taylor's assumption in the shear-layer.**

## Nomenclature

| | |
|---|---|
| $x_i$, $y_i$ | Positions. The origin is located at the center of the nozzle, in the exit plane |
| $t$ | Time |
| $U_i$ | Mean velocity field |
| $u'_i$ | Velocity fluctuation field |
| $u_i$ | Root mean square value of $u'_i$: $u_i = \sqrt{\overline{u'^2_i}}$. The overline operator stands for ensemble averaging. |
| $c_0$ | Ambiant sound speed |
| $\rho_0$ | Ambiant density |
| $M$ | Jet Mach number: $U_1(x_1 = 0, x_2 = 0)/c_0$ |
| $\epsilon$ | Viscous dissipation rate |
| $D$ | Jet diameter |
| $\delta_\theta$ | Momentum quantity |
| $\tau$ | Correlation time lag |
| $\xi_i$ | Displacement |
| $\xi_{ci}$ | Displacement of the convected frame |
| $U_c$ | Convection velocity: $\|d\vec{\xi}_c/d\tau\|$ |
| $U_a$ | Mean velocity on the jet axis: $U_1(x_1, x_2 = 0)$ |
| $M_c$ | Convection Mach number: $U_c/c_0$ |
| $R_i(\vec{x}, \vec{\xi}, \tau)$ | Correlation function: $\overline{u'_i(\vec{x}, t)u'_i(\vec{x} + \vec{\xi}, t + \tau)} \times \left[u_i(\vec{x})u_i(\vec{x} + \vec{\xi})\right]^{-1}$ |
| $\xi^+_{0i}$, $\xi^-_{0i}$, $\tau_0$ | Space and time locations of the annulation of $R_i$, the closest ones to the origin. $\xi^+_{0i} > 0$ and $\xi^-_{0i} < 0$ |
| $L^{(j)}_i(\vec{x})$ | Length scale: $(1/2)\int_{\xi^-_{0i}}^{\xi^+_{0i}} R_i(\vec{x}, \xi_j, \tau = 0)d\xi_j$ |

*Research Engineer, Département de Simulation Numérique et Aéroacoustique (DSNA), vincent.fleury@onera.fr
†Professor, Laboratoire de Mécanique des Fluides et Acoustique (LMFA), Senior Member AIAA, christophe.bailly@ec-lyon.fr
‡Professor, LMFA, Senior Member AIAA, daniel.juve@ec-lyon.fr
§Associate Professor, LMFA, marc.michard@ec-lyon.fr
¶CNRS Engineer, LMFA, emmanuel.jondeau@ec-lyon.fr

| | |
|---|---|
| $R_{Ei}(\vec{x},\tau)$ | Eulerian time correlation function: $R_i(\vec{x},\vec{\xi}=\vec{0},\tau)$ |
| $\tau_{Ei}(\vec{x})$ | Eulerian time scale: $\int_0^{\tau_{0i}} R_{Ei}(\vec{x},\tau)d\tau$ |
| $\Theta_{Ei}$ | Eulerian reference time: $L_i^{(1)}/U_1$ |
| $R_{ci}(\vec{x},\tau)$ | Time correlation function in the convected frame: $R_i[\vec{x},\vec{\xi}=\vec{\xi}_c(\tau),\tau]$ |
| $\tau_{ci}(\vec{x})$ | Time scale in the convected frame: $\int_0^{\tau_{0i}} R_{ci}(\vec{x},\tau)d\tau$ |
| $\Theta_{ci}$ | Reference time in the convected frame: $L_i^{(1)}/u_i$ |

*Subscript and superscript*

| | |
|---|---|
| 1 | Component in the axial direction |
| 2 | Component in the radial direction |

# I. Introduction

The concept of correlation is well adapted to characterize the space-time statistical properties of turbulence. The first application to aerodynamic noise has been made by Proudman[1] from the theory developed by Lighthill[2,3] to link the radiated acoustic pressure and the aeroacoustic fluctuations. To introduce the correlations of the turbulent fluctuations, Proudman estimates the acoustic intensity $I(\vec{x})$ and relates this feature to the integral over the flow domain of the fourth-order time derivative of the two-point two-time correlation of the Lighthill tensor. For isentropic, low Mach number and high Reynolds number flows, this reduces to:

$$I(\vec{x}) = \frac{1}{16\pi^2\rho_0 c_0^5}\frac{x_i x_j x_k x_l}{x^4}\int_V\int \frac{\partial^4}{\partial\tau^4}\overline{(u_i'u_j')_{\vec{y},t}(u_k'u_l')_{\vec{y}+\vec{\xi},t+\tau}}d\xi^3 dy^3$$

In this formulation, the time lag $\tau$ is connected with the displacement $\vec{\xi}$ by the relation $\tau = x - |\vec{x}-\vec{\xi}|/c_0$. The problem then reduces to the evaluation of the integration of the fourth-order velocity correlations over the flow domain. Ribner[4] tackled this problem by considering isotropic turbulence superimposed on a mean shear axisymmetric flow. The derivation of the model is not reproduced but a classical closure is to express the integrand as a function of second-order velocity correlations. In order to develop an engineering tool, a first reasonable idea is then to introduce some data provided by a $k-\epsilon$ turbulence closure in statistical models. Béchara[5] *et al.*, Bailly[6] *et al.* or Khavaran[7] among others developed such applications to subsonic and supersonic jet noise. Note that a connected and interesting discussion has recently been proposed by Morris & Farassat.[8] The expression of the space-time second-order velocity correlations takes the classical form:

$$R_i(\vec{x},\xi_j,\tau) = f\left[\frac{\xi_j}{L_i^{(j)}(\vec{x})}\right] g\left[\frac{\tau}{\tau_{Ei}(\vec{x})}\right]$$

or:

$$R_i(\vec{x},\xi_j,\tau) = f\left[\frac{\xi_j}{L_i^{(j)}(\vec{x})}\right] g\left[\frac{\tau}{\tau_{ci}(\vec{x})}\right]$$

in a convected frame. The functions $f$ and $g$ and the space-time correlation scales are usually issued from experiments or semi-empirical relations, see Ribner,[9] Goldstein[10] or Morris & Farassat[8] for instance.

Many experiments have been devoted to the measurement of the correlation scales of velocity in unstrained, homogeneous and isotropic turbulence.[11] A detailed bibliography of the pioneering investigations can be found in Comte-Bellot & Corsin.[12] In such flows, the turbulence decreases due to viscous dissipation effects only. From a dimensional analysis, Batchelor[13] and Townsend[14] have estimated the integral scales according to $\epsilon$ and $u_1$ as follows:

$$L_1^{(1)} \approx \alpha\frac{u_1^3}{\epsilon} \qquad \tau_{c1} \approx \alpha\frac{u_1^2}{\epsilon}$$

where the constant $\alpha$ has no dimension. This was confirmed experimentally by Comte-Bellot & Corsin,[15] who obtained a value of $\alpha$ close to one. In presence of a mean shear flow, turbulence decaying is mainly due to the intensity of shear. The measurements of Davies *et al.*[16] actually have shown that the integral scales $L_1^{(1)}$ and $\tau_{E1}$ in the mixing-layer of a jet depend on the local shear strain:

$$L_1^{(1)} \approx 5u_1\left(\frac{dU_1}{dx_2}\right)^{-1} \qquad \tau_{E1} \approx 3\left(\frac{dU_1}{dx_2}\right)^{-1}$$

or equivalently:

$$L_1^{(1)} \approx 0.8\delta_\theta \qquad \tau_{E1} \approx 3\frac{\delta_\theta}{U_a} \approx 5.8\frac{\delta_\theta}{U_c}$$

with $dU_1/dx_2 \approx U_a/\delta_\theta$, $u_1/U_a \approx 0.16$ and $U_c/U_a \approx 0.65$. The scaling of a characteristic time associated with the correlation function according to $U_c$ and $\delta_\theta$ is in agreement with the results found by Dimotakis & Brown[17] in a planar turbulent mixing-layer. In these pioneering investigations, the velocity fluctuations have been measured with two single hot-wires and only the correlation of the axial velocity could thus be characterized. With the development of new measurement techniques, the dataset on the correlations of velocity in jets has filled out. Hence, Lau[18] and Kerherve *et al.*[19] take advantage of the development of the Laser Doppler Anemometry (LDA) to investigate the correlation of the radial and axial components of velocity. The use of the Particle Image Velocimetry (PIV) has also allowed a global measurement of the correlations. With two coupled conventional PIV systems (dual-PIV), Bridges & Wernet[20] provides a thorough characterization of the space-time correlations of the axial and radial components of velocity in the shear-layer of subsonic jets. Ukeiley[21] explores the space correlation functions of the three components of velocity through stereoscopic single-PIV. A combined use of LDA and PIV techniques is also proposed by Chatelier & Fitzpatrick.[22]

However, in spite of the increase of amount of correlation data in jets, a fine description of the correlation scales is still needed. In the most recent studies, the evolution of the correlation scales in the shear-layer is usually given in function of the axial distance $x_1$. Owing to the earliest studies of Davies *et al.*[16] and Dimotakis & Brown,[17] these results thus depend on the specific expansion rate of the shear-layer in these experiments. Furthermore, to the authors' knowledge the characterization of the correlations of velocity on the jet axis, especially just downstream of the potential core, is still unknown.

The aim of the present work is to measure the space-time correlation scales of the axial and radial velocity components in subsonic isotherm round jets and to provide the results in function of appropriate reference features. The ratios between the space scales and between the time scales is also analysed in the light of the values expected in homogeneous and isentropic turbulence, see Batchelor[13] and Townsend.[14] The Taylor's assumption connecting the space and time scales is also discussed. A dual-PIV technique is used to explore in detail the shear-layer and the jet axis at two Mach numbers $M = 0.6$ and $M = 0.9$. The facility and the instrumentation are described in section II. The section III is devoted to the description of the one-point statistics of turbulence. The correlation length scales are provided in section IV and the correlation time scales in section V.

## II. Experimental set-up

### II.A. Facility

The experiments were performed in a facility of the Ecole Centrale de Lyon designed for acoustic testing of transonic single-stream hot jets. This facility is composed of a centrifugal compressor (maximal power of 350kW, mass-flow rate up to 1 kg.s$^{-1}$), an air drier system (power of 12kW) and of a set of controllable electric resistances (power 64kW, stagnation temperature $< 500°$ K). A nozzle of conical shape, of inlet diameter 90 mm, of exit diameter $D = 38$ mm, of inside face angle 18° and of lip thickness 2 mm is used. In this installation, Mach numbers up to 1.6 can be investigated and the static temperature can be maintained equal to the ambient temperature for $M < 1.1$. The measurement of the near-field and far-field acoustic spectra over the whole Mach number range $M < 1.6$ are found in Bogey*et al.*[23]

In the present article, the aerodynamic characterization of the jet alone is concerned. Two Mach numbers are prescribed, $M = 0.6$ and $M = 0.9$, and the temperature is controlled to get isothermal conditions. At the nozzle exit, $M$ and the static temperature are respectively maintained with less than 3% variation and 2°C according to the ambient throughout the experiments.

For the use of PIV, the jet is seeded with droplets of olive oil. Eight injectors are located in the settling portion of the wind tunnel, at 3 m upstream of the nozzle exit and spread out regularly over the circumference of the round tunnel. The injection of olive oil sprays is made through flush-wall annular slots in order to reduce flow distortion. The olive-oil droplets are produced by an home-made generator. The droplet size has been estimated by Particle Dynamics Analysis (PDA) in nearly standard thermodynamic conditions and in absence of flow and has been found to be less than 1 $\mu$m in these conditions. To measure the velocity of the ambient flow entrained and mixed in the jet core, the experimentation room is seeded with mineral oil

droplets produced by a commercial smoke generator.

### II.B. Instrumentation

The dual-PIV system consists of two coupled conventional PIV systems. Each system is composed of a pulsed double-cavity Nd:Yag laser (NewWave Solo PIV III laser or Quantel Brillant laser, wavelength of 532 nm, energy of 50 mJ/pulse, pulse length of 5 ns and operating frequency of 4 Hz) and a double-frame CCD camera (PCO SensiCam, 12 bits, $1280 \times 1024$ pixels). The laser beams are combined by an house-made optical system and then refracted by a cylindrical lens to form a light sheet (2 mm of thickness) propagating across the jet axis. The two cameras are mounted side by side and can be traversed in the axial direction over more than $15D$. A passive beamsplitter allows to visualize the same region of the jet with the two cameras. With a working distance of nearly 600mm between light sheets and cameras, and using objectives with a focal length of 60mm, a field of view of $2.2D \times 1.8D$ is obtained. The calibration is performed before operating the jet by recording simultaneously with both cameras the image of the same calibration plate. Due to the long exposure time of the second frame of CCD cameras (120 ms), a fast optical shutter is used with the first camera. Owing to the small closure delay of the shutter, the firing of both cavities of the second laser is triggered when the shutter is closed, and the second frame of the first camera is not contaminated by spurious diffused light during operation of the second PIV system. With this device, the time lag $\tau$ has been decreased down to 20 $\mu$s.

The synchronization of the two PIV systems is carried out by a commercial PIV software (Davies v7.1). The basic acquisition cycle breaks down as follows. Two conventional single-PIV acquisitions are operated successively at a time interval of $\tau$. This time lag $\tau$ is controlled by the software and has been varied from $20\mu s$ (minimal polarization time of the shutter) to 250 $\mu$s at $M = 0.9$ and 330 $\mu$s at $M = 0.6$. To obtain $\tau = 0$, the data from one single PIV system are used. The time interval between the two images required for each of the two conventional single PIV acquisitions is of 2.5 $\mu$s for $M = 0.6$ and of 1.6 $\mu$s for $M = 0.9$. After post-processing two instantaneous velocity fields time-lagged of $\tau$ are then obtained. This basic acquisition cycle is repeated at a frequency of 4Hz in order to obtain 2000 velocity field pairs.

The post-processing of the velocity maps is operated by the Davies v7.1 software after the acquisition is completed. A multipass algorithm is used, with three steps from the initial window size of $128 \times 128$ pixels to the final size of $32 \times 32$ pixels ($0.052D \times 0.052D$). Owing to a 50% overlapping of the interrogation windows, around 38 velocity vectors are measured over a distance of $1D$.

## III. Single point results

The validation of the PIV acquisition was checked in detail by comparison to other experimental techniques, see Fleury[24] for more details. The radial profiles of mean velocity and velocity fluctuations (the two components) are conform to results obtained by Laser Doppler Anemometry (LDA) and Pitot tube. The measurements are also in satisfying agreement with data found in the literature on similar high-speed jets.[25,26]

The radial profiles of mean velocity display a classical hyperbolic tangent distribution and the maximal turbulent rate of the axial and radial velocity components is of 16% and 11% respectively. The potential core length $L_c$ is of $6.5D$ for $M = 0.6$ and of $7D$ for $M = 0.6$, where $L_c$ is such that $U_1(x_1 = L_c, x_2 = 0) = 0.95U_1(x_1 = 0, x_2 = 0)$. The maximum of fluctuations on the jet axis is reached between $2.5D$ and $3.5D$ downstream of $L_c$, with $u_1/U_1(x_1 = 0, x_2 = 0) \approx 14.5\%$ and $u_2/U_1(x_1 = 0, x_2 = 0) \approx 10.5\%$ for the two jet velocities.

## IV. Space scales

The space correlation functions $R_i(\vec{x}, \vec{\xi}, \tau = 0)$ have been estimated at points $\vec{x}$ over the first eleven diameters from the nozzle exit, $x_1 < 11D$, in the shear-layer center ($x_2 = 0.5D$) and on the jet axis ($x_2 = 0$). From this dataset, the integral length scales $L_i^{(j)}(\vec{x})$ have been calculated. The results are presented in the following two sections.

### IV.A. Shear-layer

An example of the space correlation functions $R_1$ and $R_2$ obtained in the shear-layer is shown in Figure 1. This figure illustrates the quality of the PIV acquisition and of the statistical convergence of data. The complex pattern of the correlation functions $R_1$ and $R_2$ is also noticed. The contour plots of $R_1$ presents two directions along which the low-level positive correlation curves stretch out. These principal directions are distinct from the axial and radial directions and delimit four quadrants of negative correlation level, $R_1 < 0$. For $R_2$, the positive-level contours stretch out only in the radial direction and two areas of negative correlation are observed upstream and downstream of the reference point, rather on the high-speed side of the shear-layer. Further downstream $x_1 > 2D$, the contour plot of $R_1$ and $R_2$ stretch around the reference point $\vec{x}$ but the pattern is roughly similar. Other correlation patterns are available in Fleury.[24]

To illustrate the calculation of the length scales $L_i^{(1)}$, the axial distribution of the correlation functions $R_i$ at $x_1 = 2D$ is plotted in figure 2 for $i = 1$ and 2. The integration of $R_i$ is made by a classical trapezoidal method using only the experimental data and over the domain of positive $R_i$ values around the origine $\xi_1 = 0$. If $R_i$ vanishes outside of the measurement domain, the location of $\xi_{01}^-$ and $\xi_{01}^+$ is extrapolated linearly from the values taken at the neighborhood of the boundary. Note that no extrapolation function is used to calculate the length scales. A similar data analysis is carried out for the radial length scales $L_i^{(2)}$.

The evolution of the correlation length scales $L_i^{(j)}$ in the shear-layer is shown in Figure 3. Several results found in the literature are superimposed for comparison. A rather poor agreement with the pioneering results of Laurence[27] and Davies *et al.*[16] is noticed for $L_1^{(1)}$, while a satisfying agreement is found with the data of Liepmann[28] concerning $L_1^{(2)}$. The more recent data of Lau,[18] Jordan & Gervais[29] and Kerherve *et al.*[19] collapse quite better, except however for the scales $L_2^{(j)}$ based on the radial velocity.

The inspection of these results shows the linear evolution of the length scales $L_i^{(j)}$ according to the position along the shear-layer. This suggests a linear relation between $L_i^{(j)}$ and the local momentum thickness of the shear-layer $\delta_\theta$, as supported by the results displayed in Figure 4. Far enough downstream, one actually gets the remarkable relations:

$$L_1^{(1)} \approx 2\delta_\theta, \qquad L_1^{(2)} \approx \delta_\theta \qquad \text{and} \qquad L_2^{(1)} \approx \delta_\theta \tag{1}$$

Such a simple relation cannot however be provided for $L_2^{(2)}$. In the case of isotropic turbulence, the axial length scale of the axial velocity, $L_1^{(1)}$, is equal to the radial length scale of the radial velocity, $L_2^{(2)}$. In the same way, one expects the relation $L_1^{(2)} = L_2^{(1)}$ to be verified. These isotropic ratios of the integral length scales are plotted in Figure 5. We roughly found $L_1^{(2)} \simeq L_2^{(1)}$, and more scattered values for the ratio $L_1^{(2)}/L_2^{(1)}$. Furthermore the relations (1) imply:

$$L_1^{(1)}/L_1^{(2)} = 2 \tag{2}$$

which also is a requirement for isotropic turbulence, see Batchelor[13] and Townsend.[14]

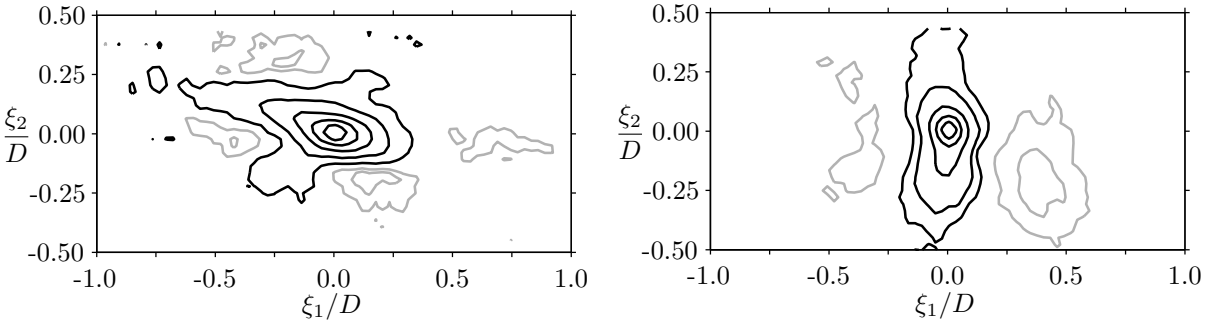


**Figure 1. Contour plot of the space correlation functions $R_1(\vec{x}, \vec{\xi}, \tau = 0)$ (left) and $R_2(\vec{x}, \vec{\xi}, \tau = 0)$ (right) in the shear-layer, at $x_1 = 2D$, $x_2 = 0.5D$ and $M = 0.9$. The $R_1$-correlation levels are 0.8, 0.6, 0.4, 0.2, 0.05 in black and -0.05, -0.1 in grey. The $R_2$-correlation levels are 0.8, 0.6, 0.4, 0.2, 0.1 in black and -0.1, -0.2 in grey.**

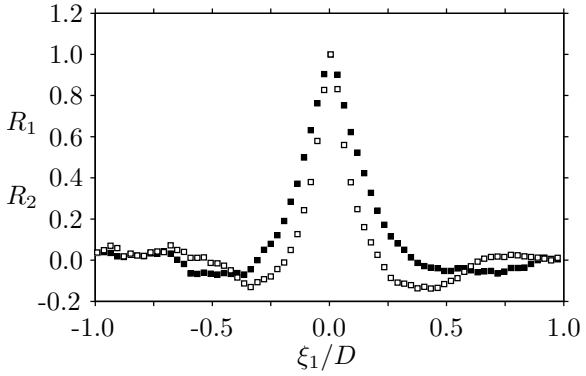


**Figure 2. Axial distribution ($\xi_2 = 0$) of the space correlation functions $R_1$ (■) and $R_2$ (□) in the shear-layer, at $x_1 = 2D$, $x_2 = 0.5D$ and $M = 0.9$.**

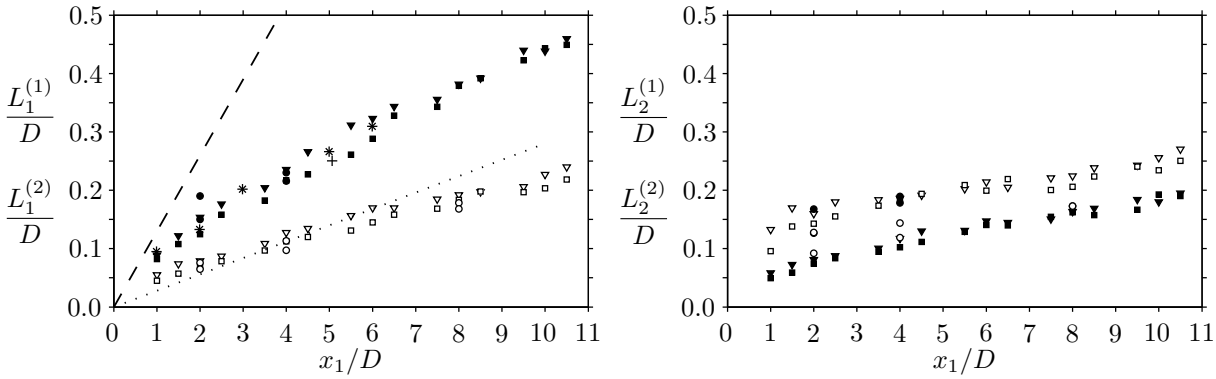


**Figure 3. Correlation length scales in the shear-layer center ($x_2 = 0.5D$) at $M = 0.6$ (▽, ▼) and $M = 0.9$ (□, ■). $\cdots$ Laurence[27] and Davies *et al.*[16] ($L_1^{(1)} = 0.13x_1$); $--$ Liepmann[28] ($L_1^{(2)} = 0.028x_1$); + Jordan[29] ($M = 0.75$); ○, ● Lau[18] ($M = 0.5$ and $M = 0.9$); $*$ Kerherve[19] (perfectly expanded jet at $M = 1.2$). The black symbols concern the axial direction, $L_i^{(1)}$. The open ones the radial direction, $L_i^{(2)}$.**

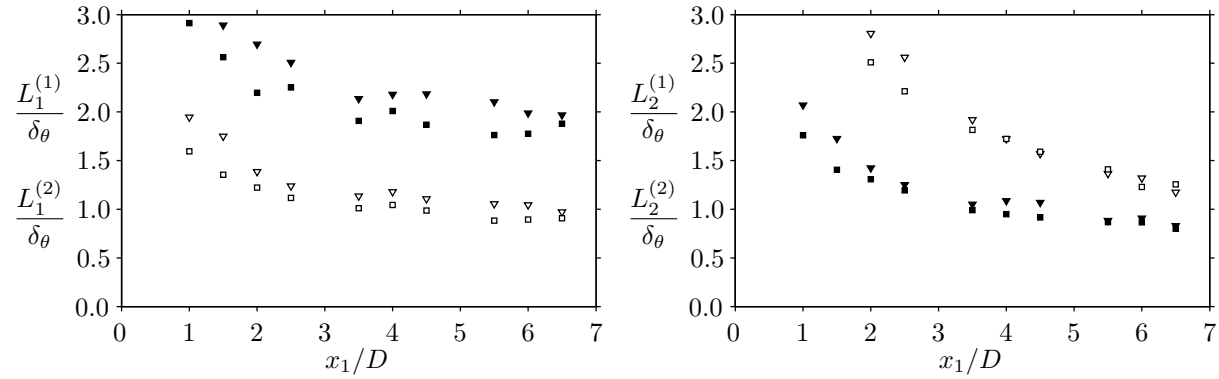


**Figure 4. Ratio between the correlation length scales in the shear-layer and the local momentum thickness $\delta_\theta$ for $M = 0.6$ and $M = 0.9$. The legend is the same as in figure 3.**

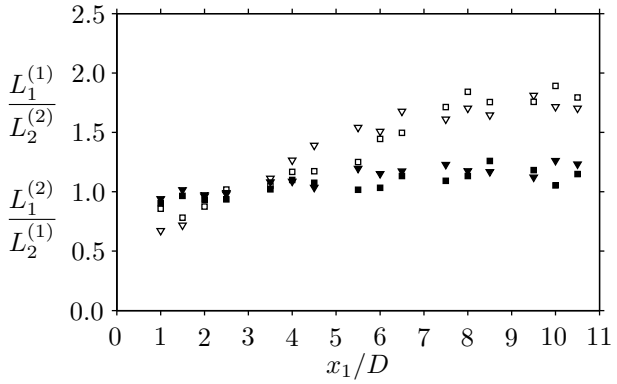


**Figure 5. Isotropic ratios between the correlation length scales in the shear-layer for $M = 0.6$ (▽, ▼) and $M = 0.9$ (□, ■). The black symbols concern $L_1^{(2)}/L_2^{(1)}$. The open ones $L_1^{(1)}/L_2^{(2)}$.**

### IV.B. Jet axis

An example of space correlation functions $R_1$ and $R_2$ obtained on the jet axis is shown in Figure 6. The contour plots of $R_1$ and $R_2$ stretch out along orthogonal directions, in the axial direction for $R_1$ and in the radial direction for $R_2$. Negative correlation areas are also noticed on the two sides of the stretching directions, *i.e.* $\xi_2 > 0$ and $\xi_2 < 0$ for $R_1$ and on the $\xi_1 < 0$ and $\xi_1 > 0$ sides for $R_2$. This type of correlation pattern has been observed all over the jet axis, far enough downstream of the potential core. At the end of the potential core, $x_1 = L_c$, the negative correlation areas of $R_1$ are turned of 90° with regard to the present illustration and are thus on the $\xi_1 < 0$ and $\xi_1 > 0$ sides, see Fleury.[24]

The integral length scales associated with $R_1$ and $R_2$ have been calculated as explained previously in IV.A. The result is plotted in figure 7. The influence of the Mach number $M$ seems negligible. Moreover the integral lengths $L_1^{(2)}$, $L_2^{(1)}$ and $L_2^{(2)}$ do not grow significantly as the reference point is moved downstream. One actually gets the following approximations:

$$L_1^{(2)} \approx 0.15D, \qquad L_2^{(1)} \approx 0.17D \qquad \text{and} \qquad L_2^{(2)} \approx 0.23D \tag{3}$$

The isotropic character of the integral length scales is investigated in figure 8. Although the isotropic ratios are not constant, they do not indicate a strong anisotropy of the integral length scales. In particular, $L_1^{(1)}/L_2^{(2)}$ is very close to unity for $x_1 > 8D$.

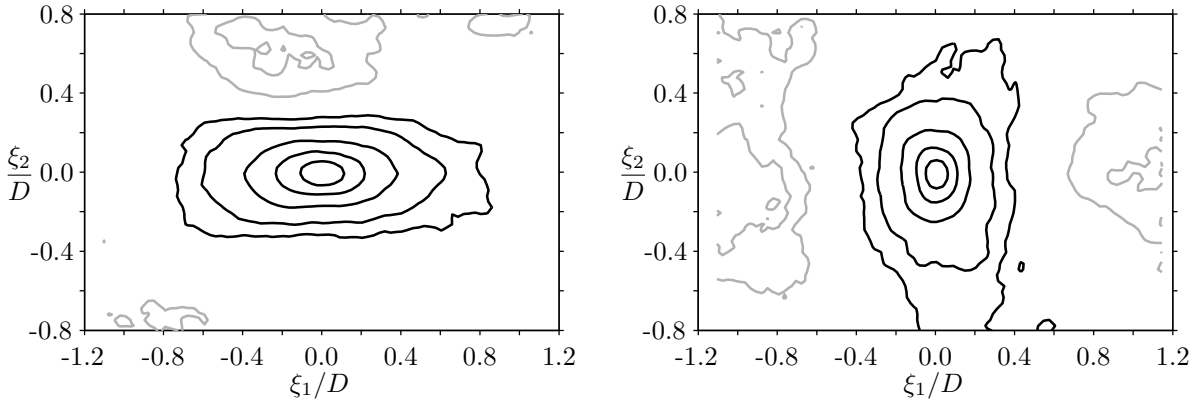


**Figure 6. Contour plots of the space correlation functions $R_1(\vec{x}, \vec{\xi}, \tau = 0)$ (left) and $R_2(\vec{x}, \vec{\xi}, \tau = 0)$ (right) on the jet axis ($x_2 = 0$) at $x_1 = 10D$ and for $M = 0.9$. The correlation levels are 0.8, 0.6, 0.4, 0.2, 0.1 in black and -0.05, -0.1 in grey.**

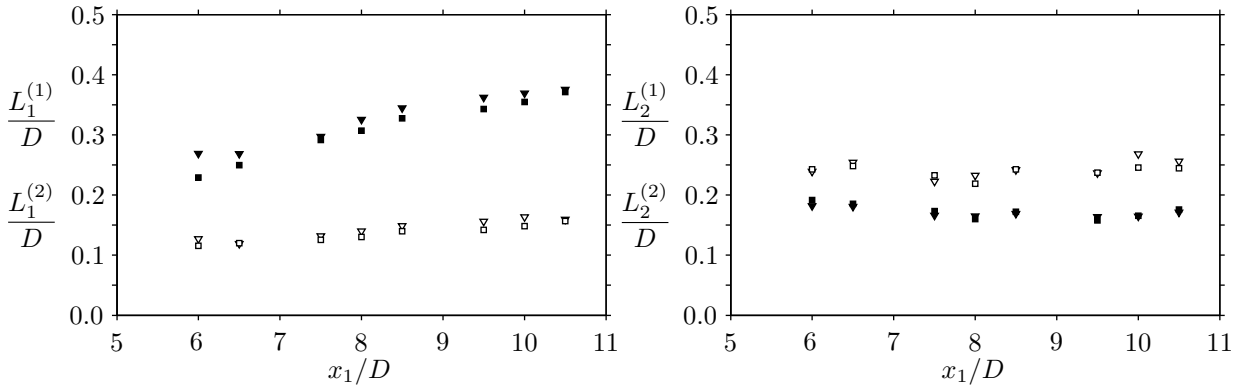


**Figure 7. Correlation length scales on the jet axis ($x_2 = 0$), for $M = 0.6$ and $M = 0.9$. The legend is the same as in figure 3.**

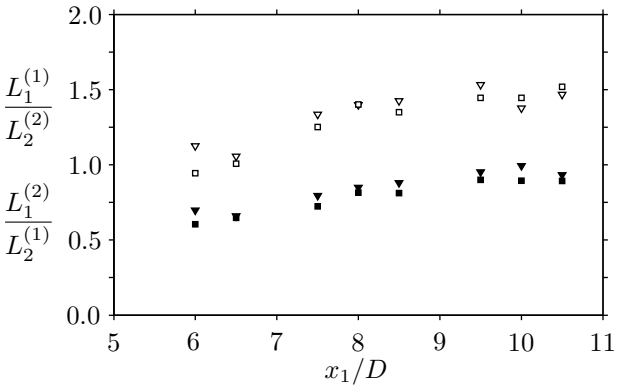


**Figure 8. Isotropic ratios between the correlation length scales on the jet axis, for $M = 0.6$ and $M = 0.9$. The legend is the same as in firgure 5.**

## V. Time scales

Due to the large amount of data required for the analysis of the time correlation functions, the space-time measurements have been limited to three areas in the shear-layer, around $x_1 = 4.5D$, $x_1 = 6.5D$ and $x_1 = 10.5D$.

As illustration, the contour plots of $R_1$ and $R_2$ in the shear-layer at $x_1 = 6.5D$ and $M = 0.9$ are displayed for different time-lags $\tau$ in Figure 9. The convection and the attenuation of the correlation patterns are clearly displayed. These effects are analysed quantitatively below.

For the same reference point and condition, $(x_1, x_2) = (6.5D, 0.5D)$ and $M = 0.9$, the location of the maximum correlation $\vec{\xi_c}$ has been followed with respect to the time-lag $\tau$. Both $R_1$ and $R_2$ have been considered. The displacement $\vec{\xi_c}$ is along the axial direction mainly. The result for $\xi_{c1}$ is provided in figure 10. As expected, the location of the maximum correlation $\xi_{c1}$ is identical for $R_1$ and $R_2$ and moves linearly according to $\tau$. From this curve, a convection velocity of the correlation pattern $U_c$ is derived. The result is provided in Table 1 for the different reference points and for the two Mach numbers. In all the cases, a convection velocity between $0.6U_a(x_1)$ and $0.7U_a(x_1)$ is found, as classically expected in the shear-layer center.

Two integral time scales are usually associated with the time-attenuation of the correlation functions. The first one, $\tau_{ci}$, is the reference time of the correlation function in the convected frame $R_{ci}(\tau)$, *i.e.* of the attenuation of the maximum correlation. The second one, the Eulerian correlation time $\tau_{Ei}$, is the characteristic time of the correlation function at the reference point $R_{Ei}(\tau)$. By definition $R_{ci}(\tau) \geq R_{Ei}(\tau)$, whence $\tau_{Ei} \geq \tau_{ci}$. To illustrate the calculation of these time scales, the example of the correlation functions $R_{ci}(\tau)$ and $R_{Ei}(\tau)$ measured in the shear-layer at $(x_1, x_2) = (6.5D, 0.5D)$ and $M = 0.9$ is plotted in Figure 11. Due to the weak levels of the correlation $R_{ci}$, below 0.5, the time-scales $\tau_{ci}$ is estimated by use of a model function of classical exponential form:

$$R_{ci} \approx \exp\left(-\frac{\tau}{\tau_{ci}}\right)$$

This function is actually a good approximation of the data and $\tau_{ci}$ is associated with the best least-mean-square approximation. The evaluation of the time-scale $\tau_{Ei}$ is obtained by the integration of the data over the positive correlation range $R_{Ei} > 0$, with linear extrapolation of the zero-correlation time eventually, as for the length scales.

The results are provided in Table 2 according to the reference times $\Theta_{ci}$ and $\Theta_{Ei}$. Following the Taylor's assumption, $\Theta_{ci}$ and $\Theta_{Ei}$ are respectively based on the local mean velocity $U_1$ and the local rms velocity $u_i$. The reference length is the correlation length $L_i^{(1)}$. From these results, one notices the remarkable relations:

$$\tau_{ci} \approx \Theta_{ci} \qquad \tau_{Ei} \approx \Theta_{Ei} \tag{4}$$

The relationships between the Eulerian time-scales and the time-scales in the convected frame is investigated in Table 3. Owing to the expression (4) and the results provided in section III, one actually expects:

$$\frac{\tau_{E1}}{\tau_{c1}} = \frac{u_1}{U_1} = \frac{u_1}{U_a}\frac{U_a}{U_1} = 0.16 \times 2 = 0.32$$

and:

$$\frac{\tau_{E2}}{\tau_{c2}} = \frac{u_2}{U_1} = \frac{u_2}{U_a}\frac{U_a}{U_1} \approx 0.11 \times 2 = 0.22$$

which is in reasonable agreement with the experimental results.

Moreover in the case of isentropic turbulence, the expression (4) implies the following relationship between the time scales associated with the radial and axial velocity components:

$$\frac{\tau_{c2}}{\tau_{c1}} = \frac{u_1}{u_2}\frac{L_2^{(1)}}{L_1^{(1)}} = \frac{L_2^{(1)}}{L_1^{(1)}} = \frac{1}{2} \tag{5}$$

and:

$$\frac{\tau_{E2}}{\tau_{E1}} = \frac{L_2^{(1)}}{L_1^{(1)}} = \frac{1}{2} \tag{6}$$

The experimental value of these ratios is given in table 3 as well. As noticed, the integral time-scales also follow closely well the requirement of isotropy, or, at least do not present a strong anisotropy.

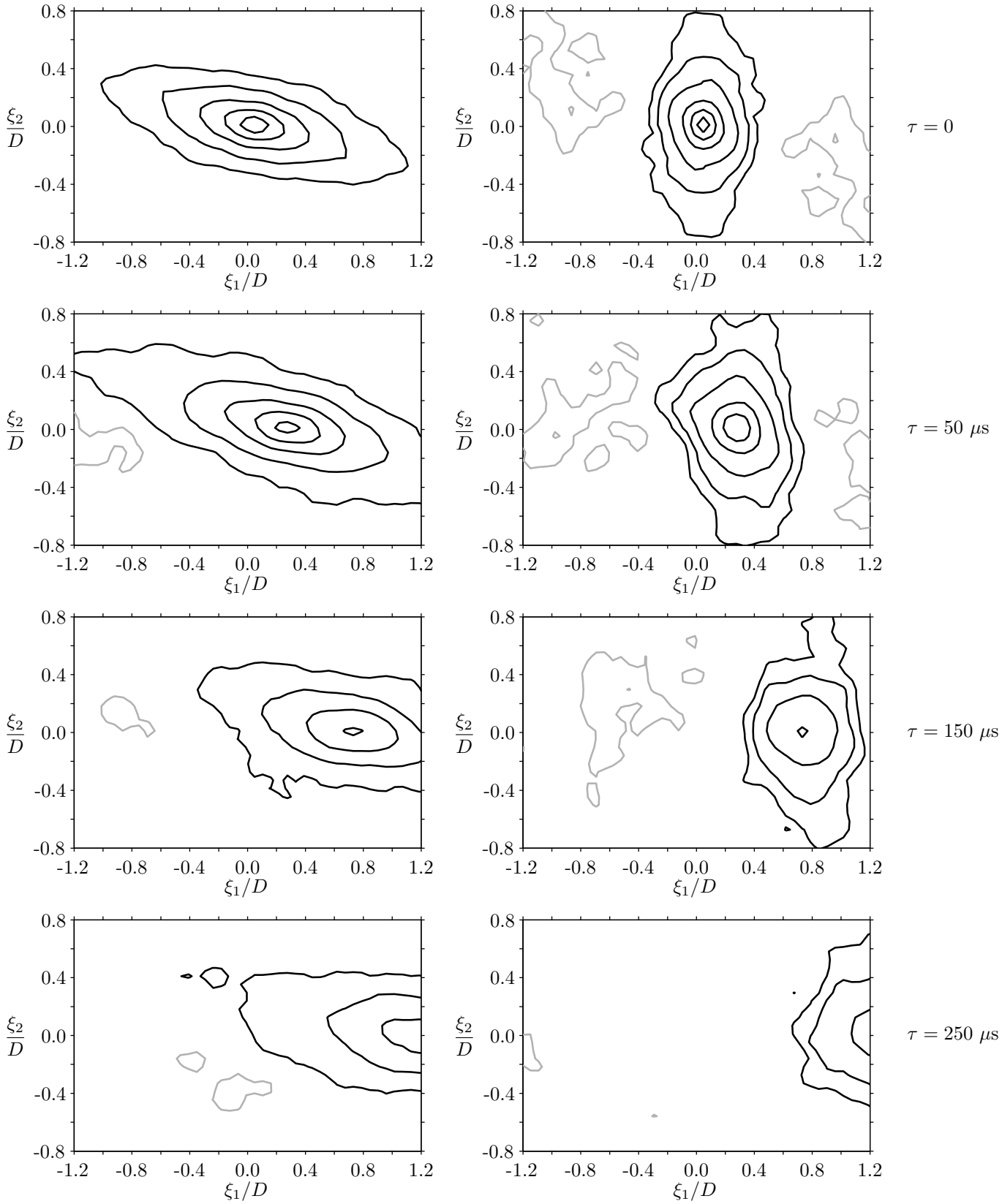


**Figure 9. Space-time correlation functions $R_1(\xi_1, \xi_2, \tau)$ (left) and $R_2(\xi_1, \xi_2, \tau)$ (right) in the shear-layer center ($x_2 = 0.5D$), at $x_1 = 6.5D$ and for $M = 0.9$. The correlation levels are 0.8, 0.6, 0.4, 0.2, 0.05 in black and -0.05, -0.1 in grey for $R_1$ and 0.8, 0.6, 0.4, 0.2, 0.1 in black and -0.1, -0.2 in grey for $R_2$.**

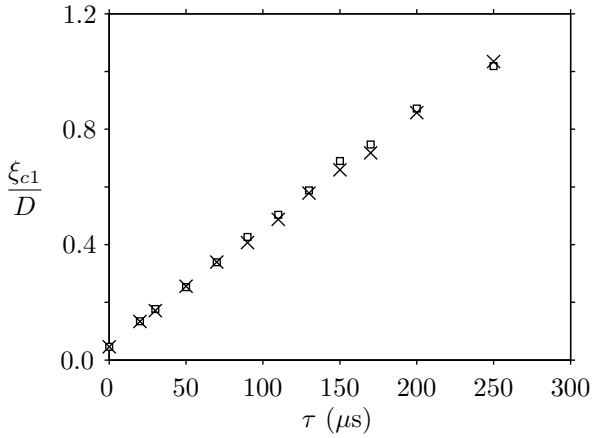


**Figure 10. Displacement of the maximum of $R_1$ (□) and $R_2$ (×) according to the delay $\tau$. The reference point $(x_1, x_2)$ is located in the shear-layer center $(6.5D, 0.5D)$ and $M = 0.9$.**

**Table 1. Convection velocity $U_c$ in the shear-layer center ($x_2 = 0.5D$).**

| $M = 0.6$ | | | $M = 0.9$ | | |
|---|---|---|---|---|---|
| $x_1$ | $U_C$ | $\frac{U_c}{U_a}$ | $x_1$ | $U_C$ | $\frac{U_c}{U_a}$ |
| $4.5D$ | - | - | $4.5D$ | 87 m.s$^{-1}$ | 0.6 |
| $6.5D$ | 55 m.s$^{-1}$ | 0.6 | $6.5D$ | 85 m.s$^{-1}$ | 0.6 |
| $10.5D$ | 49 m.s$^{-1}$ | 0.7 | $10.5D$ | 76 m.s$^{-1}$ | 0.7 |

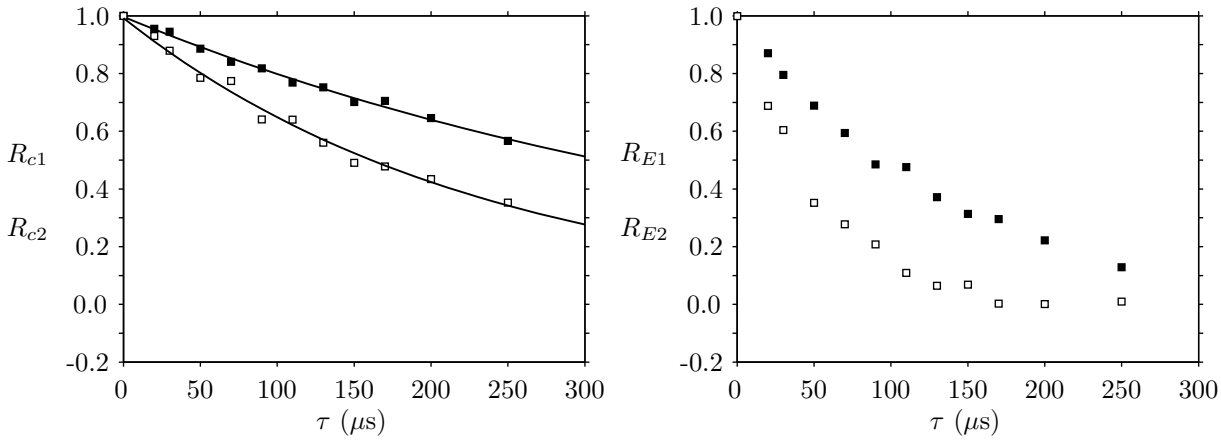


**Figure 11. Attenuation of the correlation in the shear-layer center ($x_2 = 0.5D$), for $x_1 = 6.5D$ and $M = 0.9$. The black symbols concern the axial velocity $R_{c1}$ and $R_{E1}$. The open ones, the radial velocity $R_{c2}$ and $R_{E2}$.**

**Table 2. Time-scales in the shear-layer.**

| | $x_1$ | $\tau_{c1}$ | $\frac{\tau_{c1}}{\Theta_{c1}}$ | $\tau_{c2}$ | $\frac{\tau_{c2}}{\Theta_{c2}}$ | $\tau_{E1}$ | $\frac{\tau_{E1}}{\Theta_{c1}}$ | $\tau_{E2}$ | $\frac{\tau_{E2}}{\Theta_{E2}}$ |
|---|---|---|---|---|---|---|---|---|---|
| $M = 0.6$ | $4.5D$ | - | - | - | - | - | - | - | - |
| | $6.5D$ | 511 $\mu$s | 1.2 | 260 $\mu$s | 0.90 | 121 $\mu$s | 1.1 | 56.0 $\mu$s | 1.1 |
| | $10.5D$ | 712 $\mu$s | 1.1 | 396 $\mu$s | 1.1 | 172 $\mu$s | 0.9 | 80.4 $\mu$s | 1.1 |

| | $x_1$ | $\tau_{c1}$ | $\frac{\tau_{c1}}{\Theta_{c1}}$ | $\tau_{c2}$ | $\frac{\tau_{c2}}{\Theta_{c2}}$ | $\tau_{E1}$ | $\frac{\tau_{E1}}{\Theta_{c1}}$ | $\tau_{E2}$ | $\frac{\tau_{E2}}{\Theta_{E2}}$ |
|---|---|---|---|---|---|---|---|---|---|
| $M = 0.9$ | $4.5D$ | 249 $\mu$s | 1.4 | 148 $\mu$s | 1.1 | 57.0 $\mu$s | 1.4 | 28.8 | 1.4 |
| | $6.5D$ | 329 $\mu$s | 1.3 | 168 $\mu$s | 0.99 | 77.2 $\mu$s | 1.2 | 33.6 | 1.1 |
| | $10.5D$ | 451 $\mu$s | 1.2 | 235 $\mu$s | 1.0 | 117 $\mu$s | 1.1 | 51.2 | 1.1 |

**Table 3. Ratio between the time-scales in the shear-layer.**

| $M = 0.6$ | | | | | $M = 0.9$ | | | | |
|---|---|---|---|---|---|---|---|---|---|
| $x_1$ | $\frac{\tau_{c2}}{\tau_{c1}}$ | $\frac{\tau_{E2}}{\tau_{E1}}$ | $\frac{\tau_{E1}}{\tau_{c1}}$ | $\frac{\tau_{E2}}{\tau_{c2}}$ | $x_1$ | $\frac{\tau_{c2}}{\tau_{c1}}$ | $\frac{\tau_{E2}}{\tau_{E1}}$ | $\frac{\tau_{E1}}{\tau_{c1}}$ | $\frac{\tau_{E2}}{\tau_{c2}}$ |
| $4.5D$ | - | - | - | - | $4.5D$ | 0.59 | 0.51 | 0.23 | 0.19 |
| $6.5D$ | 0.51 | 0.46 | 0.24 | 0.21 | $6.5D$ | 0.51 | 0.43 | 0.23 | 0.20 |
| $10.5D$ | 0.56 | 0.47 | 0.24 | 0.20 | $10.5D$ | 0.52 | 0.44 | 0.26 | 0.22 |

## VI. Conclusion

Dual-PIV measurements have been carried out in Mach 0.6 and Mach 0.9 isotherm single-stream jets in order to characterize the space-time (auto-)correlation scales of the radial and axial velocity components. The shear-layer center and the jet axis have been explored in detail. For providing results of general use, the integral scales are given in function of appropriate references. In the shear-layer, the length scales depend on the local momentum thickness according to the very simple relations provided in (1), except for $L_2^{(2)}$ which follows a more subtle evolution. These relations are however valid far enough downstream only, where turbulence to be well established. On the jet axis, the diameter $D$ is the appropriate reference length and the relationships found are given by the expression (3). In the shear-layer, the appropriate reference time is based on the momentum thickness and the mean or rms local velocity depending on the time scale, whether the Eulerian time scale or the time scale in the convected frame, see the expression (4). Several ratios between the radial and axial velocity correlation scales in the shear-layer have also been found in agreement with typical values obtained in isotropic and homogeneous turbulence, see the expression (2) for the length scales and the relations (5) and (6) for the time scales.

## Acknowledgments

The authors gratefully acknowledge J.-M. Perrin, N. Grosjean, P. Souchotte and P. Roland for their technical assistance.

## References

[1]Proudman, J., "The generation of noise by isotropic turbulence," *Proc. Roy. Soc. A*, Vol. 214, 1952, pp. 119.

[2]Lighthill, M. J., "On sound generated aerodynamically. I. General theory," *Proc. Roy. Soc. London*, Vol. A211, 1952, pp. 564–587.

[3]Lighthill, M. J., "On sound generated aerodynamically. II. Turbulence as a source of sound," *Proc. Roy. Soc. London*,

Vol. A222, 1954, pp. 1–32.

[4]Ribner, H. S., "Quadrupole correlations governing the pattern of jet noise," *J. Fluid Mech.*, Vol. 77, No. 3, 1976, pp. 511–529.

[5]Béchara, W., Lafon, P., Bailly, C., and Candel, S., "Application of a $k-\epsilon$ model to the prediction of noise for simple and coaxial free jets," *J. Acoust. Soc. Am.*, Vol. 97, No. 6, 1995, pp. 3518–3531.

[6]Bailly, C., Lafon, P., and Candel, S., "Subsonic and supersonic jet noise predictions from statistical source models," *AIAA Journal*, Vol. 35, No. 11, 1997, pp. 1688–1696.

[7]Khavaran, A., "Role of anisotropy in turbulent mixing layer," *AIAA Journal*, Vol. 37, No. 7, 1999, pp. 832–841.

[8]Morris, P. J. and Farassat, F., "Two-point cross correlations of turbulence and noise predictions: analysis and simulation," *AIAA Journal*, Vol. 40, No. 4, 2002, pp. 671–680.

[9]Ribner, H. S., "On spectra and directivity of jet noise," *J. Acoust. Soc. Am.*, Vol. 35, 1963, pp. 614–616.

[10]Goldstein, M. E. and Rosenbaum, B., "Effect of anisotropic turbulence on aerodynamic noise," *J. Acoust. Soc. Am.*, Vol. 54, 1973, pp. 630–645.

[11]Bailly, C. and Comte-Bellot, G., *Turbulence*, No. ISBN 2-271-06008-7, CNRS éditions, 2003.

[12]Comte-Bellot, G. and Corrsin, S., "The use of a contraction to improve the isotropy of grid-generated turbulence," *J. Fluid Mech.*, Vol. 25, No. 4, 1966, pp. 657–682.

[13]Batchelor, G. K., *The theory of homogeneous turbulence*, Cambridge university press, 1953.

[14]Townsend, A. A., "The measurement of double and triple correlation derivatives in isotropic turbulence," *Proc. Camb. Phil. Soc.*, Vol. 43, 1947, pp. 560.

[15]Comte-Bellot, G. and Corrsin, S., "Simple Eulerian time correlation of full- and narrow-band velocity signals in grid-generated, 'isotropic' turbulence," *J. Fluid Mech.*, Vol. 48, No. 2, 1971, pp. 273–337.

[16]Davies, P. O. A. L., Fisher, M. J., and Barratt, M. J., "The characteristics of the turbulence in the mixing region of a round jet," *J. Fluid Mech.*, Vol. 15, 1962, pp. 337–367.

[17]Dimotakis, P. E. and Brown, G. L., "The mixing layer at high Reynolds number: large-structure dynamics and entrainment," *J. Fluid Mech.*, Vol. 78, No. 3, 1976, pp. 535–560.

[18]Lau, J. C., "Laser velocimeter correlation measurements in subsonic and supersonic jets," *J. Sound Vib.*, Vol. 70, No. 1, 1980.

[19]Kerhervé, F., Jordan, P., Gervais, Y., Valière, J.-C., and Braud, P., "Two-point laser Doppler velocimetry measurements in a Mach 1.2 cold supersonic jet for statistical aeroacoustic source model," *Exp. Fluids*, Vol. 37, 2004, pp. 419–437.

[20]Bridges, J. and Wernet, M. P., "Measurements of the aeroacoustic sound source in hot jets," *AIAA Paper*, 12–14 may 2003.

[21]Ukeiley, L., Mann, R., Tinney, C., and Glauser, M., "Spatial correlations in a transonic jet," *AIAA Paper*, 2004.

[22]Chatellier, L. and Fitzpatrick, J., "Spatio-temporal correlation analysis of turbulent flows using global and single-point measurements," *Exp. in Fluids*, Vol. 38, 2005, pp. 563–575.

[23]Bogey, C., Barré, S., Fleury, V., Bailly, C., and Juvé, D., "Experimental study of the spectral properties of near-field and far-field jet noise," *Int. J. Aeroacoustics*, Vol. 6, No. 2, 2007.

[24]Fleury, V., *Superdirectivité, bruit d'appariement et autres contributions au bruit de jet subsonique*, Ph.D. thesis, Ecole Centrale de Lyon (France), 2006.

[25]Lau, J. C., Morris, P. J., and Fisher, M. J., "Measurements in subsonic and supersonic free jets using laser velocimeter," *J. Fluid Mech.*, Vol. 93, No. 1, 1979, pp. 1–27.

[26]Jordan, P., Gervais, Y., Valière, J. C., and Foulon, H., "Jet exhaust aerodynamics and noise," *E.U. Research Program Jean*, Vol. Deliverable 3.4, Contract No. G4RD-CT-2000-00313, 2002.

[27]Laurence, J. C., "Intensity, scale, and spectra of turbulence in mixing region of free subsonic jet," *NACA*, Vol. 1292, 1957.

[28]Liepmann, H. W. and Laufer, J., "Investigations of free turbulent mixing," *NACA TN 1257*, 1947.

[29]Jordan, P. and Gervais, Y., "Modelling self- and shear-noise mechanisms in inhomogeneous, anisotropic turbulence," *J. Sound Vib.*, Vol. 279, 2005, pp. 529–555.